ELSEVIER

NeuroImage

www.elsevier.com/locate/ynimg
NeuroImage 39 (2008) 1246–1256

An investigation of statistical power for continuous arterial spin labeling imaging at 1.5 T

Iris Asllani,[e,*] Ajna Borogovac,[a] Clinton Wright,[b] Ralph Sacco,[b,c] Truman R. Brown,[a,e] and Eric Zarahn[d]

[a] *The Department of Biomedical Engineering, Columbia University College of Physicians and Surgeons, 630 West 168th Street, Columbia University, New York, New York 10032, USA*
[b] *The Department of Epidemiology, Columbia University College of Physicians and Surgeons, 630 West 168th Street, Columbia University, New York, New York 10032, USA*
[c] *The Department of Neurology, Columbia University College of Physicians and Surgeons, 630 West 168th Street, Columbia University, New York, New York 10032, USA*
[d] *The Department of Psychiatry, Columbia University College of Physicians and Surgeons, 630 West 168th Street, Columbia University, New York, New York 10032, USA*
[e] *The Department of Radiology, Columbia University College of Physicians and Surgeons, 630 West 168th Street, Columbia University, New York, New York 10032, USA*

Received 26 April 2007; revised 15 October 2007; accepted 16 October 2007
Available online 24 October 2007

Variance estimates can be used in conjunction with scientifically meaningful effect sizes to design experiments with type II error control. Here we present estimates of intra- and inter-subject variances for region of interest (ROI) from resting cerebral blood flow (CBF) maps obtained using whole brain, spin echo echoplanar (SE-EPI) continuous arterial spin labeling (CASL) imaging on 52 elderly subjects (age = 70.5 ± 7.9 years, 29 males). There was substantial intrasubject systematic variability in CBF of gray matter ROIs corresponding to a range of standard deviations = [39–168] (ml/(100 g min)). This variability was mainly due to two factors: (1) an expected inverse relationship between ROI volume and intrasubject variance and (2) an increased effective post-labeling delay for more superior slices acquired later in the sequence. For example, intrasubject variance in Brodmann area 4 (BA 4) was ~8 times larger than in hippocampus, despite their similar gray matter volumes. Estimated ROI-wise power was computed for various numbers of acquired CBF images, numbers of subjects, and CBF effect sizes for two experimental designs: independent sample *t*-test and paired *t*-test. The theoretical effects of pulse sequence and field strength on general applicability of these results are discussed.

Keywords: ASL; CBF; fMRI; Statistical power; Intersubject variance; Intrasubject variance

Introduction

Cerebral blood flow (CBF) is widely accepted as a physiological correlate of brain metabolic activity. Therefore, methods of measuring regional CBF, such as H_2O^{15} positron emission tomography (PET), dynamic contrast enhanced (DCE) MRI and arterial spin labeling (ASL) MRI are important tools in studying brain pathology (Alsop et al., 2000; Brunet et al., 2003; Dieterich et al., 2005; Golay et al., 2004) as well as normal brain function (Kim and Ugurbil, 1997; Wang et al., 2003a). Measurement of CBF with ASL offers several practical and scientific advantages over PET and DCE methods (Alsop et al., 2000). Although different implementations of ASL have been developed, they are all based on the principle of the indicator dilution theory of Kety and Schmidt (1948) with the modification that an endogenous tracer (arterial water) is used instead of an exogenous one. Differences between ASL methods consist of the way the water is labeled and as such they are generally classified as continuous ASL (CASL) or pulsed ASL (PASL) (Golay et al., 2004). Here we present data from CASL. In CASL, CBF is calculated from the difference between a labeled and control image. The labeled image is acquired with arterial water spins adiabatically inverted at a plane inferior to the imaging volume using a relatively long off-resonance RF pulse in the presence of a constant gradient in the direction of the flow. The control image is acquired using the same gradient but with a sine-modulated RF pulse to ideally produce no net magnetic inversion of the spins (Alsop and Detre, 1998). Each labeled and control pair is transformed to a single CBF map using a physical model and a set of measured or assumed MR parameters such as tissue and arterial T_1 (Alsop and Detre, 1996; Golay et al., 2004). In general, CASL has

* Corresponding author. Fax: +1 212 342 5773.
E-mail address: ia2026@columbia.edu (I. Asllani).
Available online on ScienceDirect (www.sciencedirect.com).

1053-8119/$ - see front matter © 2007 Elsevier Inc. All rights reserved.
doi:10.1016/j.neuroimage.2007.10.015

been shown to have a higher inherent signal-to-noise ratio (SNR) and lower sensitivity to vascular transit time errors in multi-slice acquisition compared to PASL (Wang et al., 2002). However, CASL is technically more challenging to implement mainly due to its hardware requirement for long RF pulses.

Several reports of error analysis in CASL have shown that it has very attractive statistical prospects relative to BOLD fMRI for experiments involving comparison of conditions over long time scales (Floyd et al., 2003; Wang et al., 2003a). However, little quantitative work has been reported with regard to statistical power (1—type II error rate). This is a concern because failure to control power leads to uninterpretable negative results. While in BOLD fMRI power is often neglected due to the lack of well-defined physiological units in which to express scientifically meaningful effect sizes (Zarahn and Slifstein, 2001), CASL yields CBF measurement in physiological units. In addition to meaningful CBF effect sizes, power calculations would also require specification of intra- and intersubject CASL CBF variances. Here, intrasubject variance is defined (see Appendix) as the variation over repeated measures within the same subject over several minutes, and reflects measurement noise from the subject and MR scanner as well as physiological nuisance sources such as cardiac pulsatility and motion. Intersubject variance is defined (see Appendix) to include the variation in true CBF among subjects combined with any subject specificity in the systematic error of CASL CBF modeling such as misspecification of relaxation times. As such, intra- and intersubject variances reflect different sources of variation. Floyd et al. (2003) have reported CASL intrasubject variance estimates in ROIs from a young population. However, statistical power itself was not explicitly considered, intersubject variance (required for power analysis when comparing resting flow between different populations) was not estimated, and the ROIs were defined by vascular territory and not by neuroanatomical or functional significance.

The main purpose of this study was to estimate intrasubject (σ_ε^2) and intersubject (σ_ω^2) variances of CASL CBF in a normal elderly population in ROIs defined by neuroanatomical criteria in a standard brain space. These estimates were then used to generate example power curves for select ROIs. The independent variables of the power curves were CBF effect size, number of acquired CBF images per subject, and number of subjects. The two fundamental ANOVA designs for which ROI-wise power was investigated were independent sample *t*-test (which allows comparison of CBF for a given state between two populations) and paired *t*-test (which allows comparison of CBF between two conditions within a population).

Controlling type II error leads to great savings of financial, researcher and patient resources by ensuring that CASL CBF experiments will provide meaningful results. Our population of interest was elderly subjects, making the results highly relevant for studies of Alzheimer's disease (AD) and other age-related diseases.

Materials and methods

Subjects demographics

Resting CBF values were obtained from CASL images from subjects ($N' = 52$ years of age: 70.5 ± 7.9 (mean ± SD), 29 males) that were randomly sampled from the MRI substudy cohort of the Northern Manhattan Study (NOMAS), a prospective community-based sample of a stroke-free population. Details of subject recruitment methods, demographics, and inclusion/exclusion criteria have been previously described (Sacco et al., 2004). Briefly, subjects were enrolled into the MRI substudy using the following criteria: (1) age older than 55, (2) no contraindications to MRI, (3) provided written consent as approved by the Columbia University Institutional Review Board. Because this study was part of a larger study, the total scanning time was 45 min, 5 of which were spent on acquisition of CASL and 10 on acquiring the high-resolution T_1-weighted structural image.

MRI acquisition parameters

SE-EPI CASL images were acquired on a 1.5-T Philips Intera scanner with: labeling duration = 2000 ms, post-labeling delay (PLD) = 800 ms, TE/TR = 35 ms/5000 ms, flip angle = 90°, acquisition matrix 64 × 58, in-plane resolution = 3.4 × 3.4 mm^2, slice thickness/gap = 7.5 mm/1.5 mm gap, number of transaxial slices = 15. Slices were acquired in ascending mode (i.e., inferior to superior) with slice acquisition time = 64 ms. Total number of CBF images (i.e., control/label pairs) per subject was 30.

To induce the flow-driven adiabatic inversion (labeling) of the water spins, a "block-shaped" RF pulse 2000 ms long and 3.5 μT amplitude in the presence of a *z*-gradient 2.5 mT/m was applied prior to acquisition of each labeled image (Alsop and Detre, 1998). To correct for off-resonance effects, an amplitude modulated (sinusoidal, 250 Hz) RF pulse of the same power and gradient was applied prior the acquisition of each control image (Alsop and Detre, 1998). The frequency offset of both RF pulses was set to position the labeling plane 40 mm inferior to the lower edge of the imaging volume.

To spatially normalize images into standard space, a high-resolution, T_1-weighted, 3D spoiled gradient image (SPGR) was acquired in each subject with: TE/TR = 3 ms/34 ms, flip angle = 45°, acquisition matrix = 256 × 256 × 124, voxel size = 0.94 mm × 0.94 mm × 1.29 mm.

MRI data processing

Preprocessing

Image preprocessing was implemented using SPM99 software (Wellcome Department of Cognitive Neurology) and other code written in MATLAB (Mathworks, Natick, MA). For each subject, images were preprocessed as follows: (1) all control and labeled SE-EPI images were realigned to the first control image acquired. (2) The SPGR was coregistered with the first acquired SE-EPI image using the mutual information coregistration algorithm in SPM99. (3) The coregistered SPGR was then used to determine parameters (7 × 8 × 7 non-linear basis functions) for transformation into a Talairach standard space (Talairach, 1988) defined by the Montreal Neurologic Institute (MNI) template brain supplied with SPM99. (4) This transformation was then applied to the SE-EPI images, which were re-sliced using sinc interpolation to 2 mm × 2 mm × 2 mm.

Segmentation of structural data

SPM99 was used to segment the structural image of each subject into gray matter (GM), white matter (WM), and CSF posterior probability images needed for masking and computation of CBF. These images were used in the subsequent computation of CBF and in obtaining subject-specific masks. For each subject, two types of masks were made: an EPI mask which included only voxels with SE-EPI intensity > 0.80 of the image mean and therefore contained contributions from GM, WM, and CSF, and a GM mask, which was

based on each subject's GM posterior probability image including only voxels that satisfied $P[\mathrm{GM}]>0.80$. We are using the $P[\mathrm{GM}]$ as a probabilistic measure of relative GM volume; this is justified by the fact that the expected value of CBF for a voxel with a given $P[\mathrm{GM}]$, $P[\mathrm{WM}]$, and $P[\mathrm{CSF}]$ is the same as that for a single voxel with those relative tissue volumes.

CBF computation

The spatially normalized SE-EPI images were used to compute CBF at each voxel using the two-compartment formula derived by Alsop and Detre (1996) and later modified by Wang et al. (2002):

$$\mathrm{CBF}=\left(\frac{M_c-M_l}{M_c}\right)\left(\frac{\lambda}{2\alpha}\right)\times\left\{\begin{array}{l}T_{1a}\left[e^{-w/T_{1a}}-e^{(\min[\delta-w,0]-\delta)/T_{1a}}\right]\\+e^{-\delta/T_{1a}}\left[\begin{array}{l}T_{1rf}e^{-w/T_l}\left(1-e^{\min[\delta-\tau,0]/T_{1rf}}\right)\\+T_l\left(e^{\min[\delta-w,0]/T_l}-e^{-w/T_l}\right)\end{array}\right]\end{array}\right\}^{-1}\quad(1)$$

The following parameter notation and values were used: (T_1 of blood) $T_{1a}=1400$ ms; (blood/tissue water partition) $\lambda=0.9$ ml/g; (tissue transit time) $\delta=2000$ ms; (labeling duration) $\tau=2000$ ms; (tissue T_1 in the absence of RF) $T_1=1150$ ms and 800 ms for GM and WM, respectively; (T_1 in presence of RF) $T_{1rf}=750$ ms and 530 ms for GM and WM, respectively (Alsop and Detre, 1998); (labeling efficiency for CASL at 1.5 T Philips Intera) $\alpha=0.70$ (Werner et al., 2005). For each voxel, CBF was calculated as a sum of GM, WM, and CSF contributions weighted by the voxel's posterior probability of each tissue type. For each slice, the effective PLD, w, was adjusted to account for the slice acquisition time: $w=$ (acquisition slice #-1) (64 ms)$+800$ ms. An assumption of Eq. (1) is that $\tau+w>\delta$ which we assume is satisfied in our experiment given the range of δ reported in the literature (1.0–1.6 s) (Mildner et al., 2005; Wang et al., 2003b).

ROI selection

To maximize inter-laboratory generalizability of our findings, a publicly available ROI software library (wfu_pickatlas (Maldjian et al., 2004; Maldjian et al., 2003; Tzourio-Mazoyer et al., 2002)) was used. Seven ROIs per hemisphere (14 total) were selected in MNI space in three-dimensional mode: hippocampus, inferior frontal gyrus, middle frontal gyrus, occipital lobe, precentral gyrus, Brodmann area (BA) 4, temporal lobe. These ROIs were selected because they have been considered in studies of aging of the brain as well as age-related pathologies (Alsop et al., 2000; Scarmeas et al., 2004). Moreover, we chose ROIs with substantial variation in size and anatomical location to account for the effect on estimated variances of ROI volume, arterial transit time (δ_a), and effective PLD (w), which increases with slices acquired later in the acquisition.

PLD experiment

An underlying assumption of Eq. (1) is $w>\delta_a$ (Wang et al., 2002). To test this assumption, CASL images were acquired on a single random subject from the cohort (66-year-old female) at multiple PLD values (100 to 1500 ms, step of 100 ms). Percent change maps $[(M_c-M_l)/M_c]$ maps were computed for the intersection of this subject's GM mask and each acquisition slice. To minimize the effect of motion, only voxels belonging to the same acquisition slice for all images were analyzed; i.e., if, due to motion, a voxel that was at a given slice for a given PLD acquisition had shifted to an adjacent slice in another PLD acquisition, that voxel was not included. Due to the time constraint of this experiment, only 9 slices (approximately positioned as slices 7–15 in the imaging volume of the main experiment) and 20 CASL images were acquired for each PLD. Otherwise, all other acquisition parameters and processing procedures were identical to the main experiment. δ_a and CBF for each slice were estimated from the best fit of the theoretical one-compartment vascular model of Buxton et al. (1998, see Eq. (5)) to the percent change values.

Slice acquisition ordering effect

To test the effect of acquisition order on the validity of CBF measurement, CASL images were acquired on a young volunteer (26-year-old, female) in both ascending and descending order. The w for the slice of interest (chosen near the top of the brain) was fixed at 1640 ms for both ascending and descending modes, thus obviating any effect of w in the error measurement. All other acquisition parameters and image processing were the same as in the main experiment. Slice-wise mean CBF and σ_ε^2 were estimated for both acquisition orders.

Power analysis

ROI-wise power analyses for independent samples and paired t-tests required estimation of σ_ε^2 and σ_ω^2 (see Appendix for computational details). The ROI-wise variances were estimated for both GM and EPI masks using conjunction of CBF image, ROI, and the respective mask. Note that the ROI-wise variance calculations involved not the variation in CBF measurements among voxels within the ROI but rather the variation in the ROI CBF average over repeated measurements or subjects (see Appendix). Also, to keep $\hat{\sigma}_\omega^2>0$, any negative values originating from its computation (Eq. (A10)) were set to zero.

While we present estimates of σ_ε^2 and σ_ω^2 for all ROIs and for both masking procedures, in the interest of concision, we restricted presentation of estimated power results to only two GM ROIs, left hippocampus and left BA 4. (Results for the right hemisphere and/or SE-EPI masking were very similar.) These ROIs were selected because they have similar size but substantially different z-coordinates, therefore providing variability in w which is expected to affect noise. Furthermore, each is of immediate interest to one of the two design types: hippocampus for an independent sample t-test in the context of AD (Scarmeas et al., 2004) and BA 4 for a paired t-test in the context of motor execution. For these two ROIs, power was computed for both experimental designs with two-tailed $\alpha=0.05$ for various values of N (# of subjects per group) and n (# of observations per subject). N and n are not to be confused with N' and n' (see Appendix). Effect sizes of $\mu=10$ and 20 ml/(100 g min) were assumed. These values of μ were selected to represent small and moderate CBF effect sizes (Kim and Ugurbil, 1997).

Results

CASL CBF measurements

To provide a qualitative sense of the images on which the analysis was based, group mean SPGR and CASL CBF images are

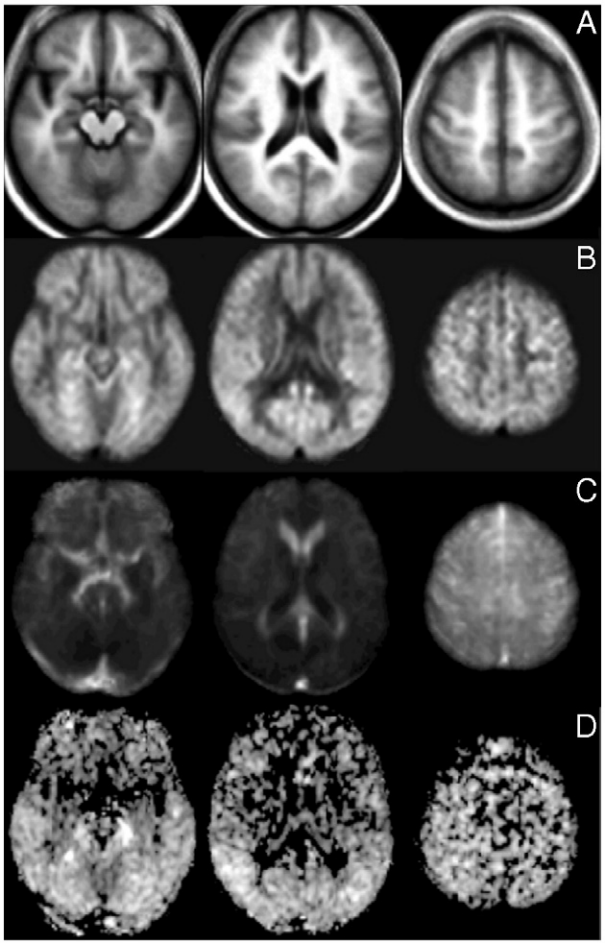

Fig. 1. Images of SPGR (A), CASL CBF (B), estimated intrasubject variance, $\hat{\sigma}^2_\varepsilon$(C), and estimated voxel-wise intersubject variance, $\hat{\sigma}^2_\omega$ (D). Panels A–C show images averaged across all subjects. Note good coregistration and spatial normalization. MNI *z*-coordinates of the slices shown are 19, 35, 53, and were chosen to represent lower, middle, and upper brain, containing portions of hippocampus, lateral ventricles, and BA 4, respectively. (Note that the negative values in panel D were zeroed to keep $\sigma^2_\omega > 0$.)

shown in Figs. 1A and B, respectively. Visual inspection shows a general lack of strong intravascular signal as well as good tissue contrast of the CBF signal (Fig. 1B). Fig. 2 provides a quantitative description of GM CBF group mean values versus acquisition slice. The range of slice-wise CBF values [49–77 ml/(100 g min)] is in reasonable agreement with what has been reported for non-partial volume corrected GM CBF with PET (Kudo et al., 2003) and ASL (Golay et al., 2004).

There is an evident pattern in the CBF versus acquisition slice (Fig. 2). This pattern could reflect a property of true CBF, GM density, or a bias inherent in the CASL model used. The variation of mean $P[\mathrm{GM}] > 0.8$ and $P[\mathrm{WM}] > 0.8$ across slices was 2% and 6%, respectively, and therefore cannot account for the ~26% slice-wise variation seen in CBF (Fig. 2).

Figs. 1C and D are maps of $\hat{\sigma}^2_\varepsilon$ (pooled over subjects) and $\hat{\sigma}^2_\omega$, respectively. Note that there is no theoretical reason why high $\hat{\sigma}^2_\varepsilon$ implies the presence of CBF; comparison of sagittal sinus signal between Figs. 1B and C shows a lack of CBF signal even in the presence of high $\hat{\sigma}^2_\omega$ (which we believe is due to variations in intensity in the SE-EPI images due to the slow flow in the sagittal

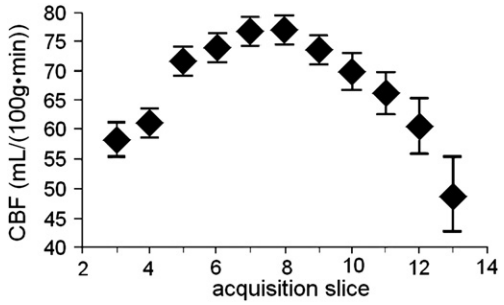

Fig. 2. Plot of GM CBF versus slice acquisition number. Only slices having usable data from all subjects ($N' = 52$) are shown. Error bars represent ±1 SEM across subjects.

sinus). Conversely, high σ^2_ω (Fig. 1D) is expected to co-localize with CBF; comparison of Figs. 1B and D bears this out. Also note the general increase in $\hat{\sigma}^2_\varepsilon$ as one moves superiorly.

Effect of PLD

An underlying assumption in Eq. (1) is that $w > \delta_a$ (Alsop and Detre, 1996; Wang et al., 2002). To validate this assumption, δ_a was estimated by acquiring CASL images at varying PLD values as described in 'Materials and methods'. Fig. 3 shows the dependence of percent change signal on w for each acquisition slice with the solid line representing the best fit. The estimated δ_a ranged from 333 to 1068 ms, increasing linearly with ascending slice position (slope = 122 ms/cm). For all slices, $w - \delta_a > 500$ ms. Furthermore, since the first slice acquired in our main CBF dataset was approximately 5 cm inferior to the one in this experiment, this provides an estimated lower bound on the satisfaction of $w > \delta_a$. However, careful inspection of Fig. 1B shows the presence of some high intravascular signal, which means that the above condition was most likely not fulfilled for all the subjects.

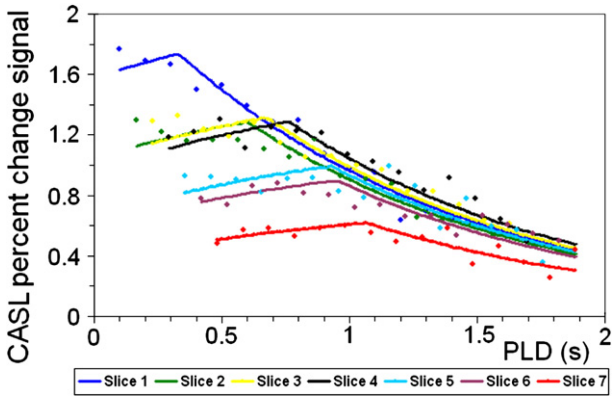

Fig. 3. Plots of GM CASL percent change signal from each acquisition slice versus w from a single elderly subject. Small circles indicate the actual data points whereas solid lines represent the best fit. Data from each acquisition slice are color coded with the most inferior slice (blue, corresponding approximately to slice 7 of the main experiment), and the most superior slice (red, corresponding approximately to slice 13 of the main experiment.) Each plot is shifted by 64 ms (slice acquisition time) relative to the previous one with the most superior slice (red) having the longest w values. Only slices having usable data from all PLDs are shown.

Effect of slice acquisition order

Theoretically, for an ascending acquisition order, $w > \delta_a$ implies no saturation of labeled spins destined for the imaged slice, further implying that computed CBF is independent of acquisition order. To validate this reasoning, we acquired CBF images using both ascending and descending acquisition orders with w fixed at 1640 ms for a slice of interest near the top of the brain (where the saturation effect would be more prominent). The estimated CBF values in GM of that slice were 47.0 and 50.9 ml/(100 g min), for ascending and descending acquisition order, respectively. This difference was not significant [$t(56) = -0.60$, $p = 0.55$].

Power analysis

Normality of CASL CBF distribution

The power analysis in this study formally assumes that errors are normally distributed. In practice, except for highly non-normal errors, the theory is expected to hold well in approximation due to the central limit theorem. For qualitative inspection, sample histograms of the ROI means for left hippocampus (Fig. 4A) and left BA 4 (Fig. 4B) are provided as representative.

To quantitatively test for any evidence of non-normality, we estimated the skewness (S) and kurtosis (K) (computed such that their expectation equals zero for a normal density) of the ROI-wise CBF distribution across subjects ($N' = 52$). In all ROIs, the 95% confidence intervals for both S and K contained zero.

If the underlying voxel-wise distributions deviate sufficiently from normal, $|S|$ and/or $|K|$ would be expected to increase as ROI volume decreases. However, if strong spatially coherent non-normal noise sources are present, $|S|$ and/or $|K|$ would be expected to increase as ROI volume increases. For all our ROIs, the estimated correlations between either $|S|$ or $|K|$ with ROI volume were not significant (two-tailed $P > 0.10$ for all). This result suggests that neither non-normal voxel-wise distributions or non-normal spatially coherent noise sources are appreciable in CASL CBF measurements for the ROIs examined.

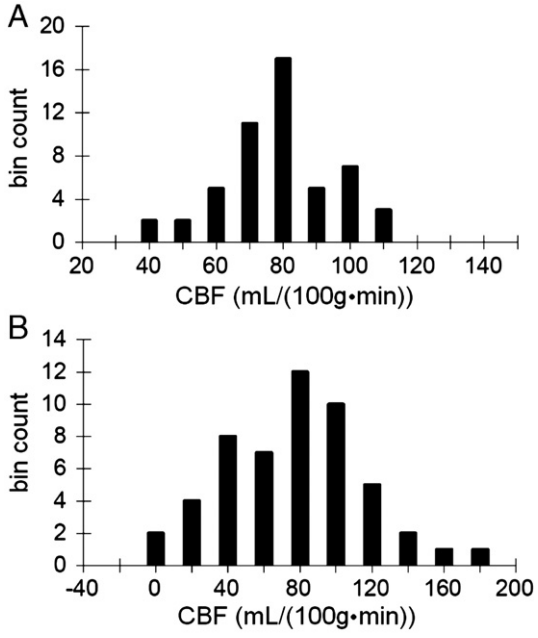

Fig. 4. Histograms of GM ROI-wise CBF averages for (A) left hippocampus and (B) left BA 4. (One value per subject, each of the temporal average of 30 CBF observations.)

ROI-wise variances

Table 1 shows $\hat{\sigma}^2_\varepsilon$ and $\hat{\sigma}^2_\omega$ for all ROIs for both GM and SE-EPI masking procedures. CBF, $\hat{\sigma}^2_\varepsilon$, and $\hat{\sigma}^2_\omega$ were each highly correlated between the two masks employed ($R = 0.74$, 0.99 and 0.94, respectively). Within each masking procedure, $\hat{\sigma}^2_\varepsilon$ and $\hat{\sigma}^2_\omega$ were also positively correlated ($R = 0.61$ and 0.72 for GM and SE-EPI masking, respectively), which was unexpected. A possible explanation for at least some component of this correlation is that only a single value of tissue transit time, δ was used for CBF computation for all slices. However, δ would be expected to vary approximately linearly with δ_a if one thinks of it as simply the sum of arterial transit time, δ_a, plus the time it takes labeled water to diffuse into the tissue. Assuming a uniform δ could introduce a scaling error into CBF computation, which would contribute a positive covariance between $\hat{\sigma}^2_\varepsilon$ and $\hat{\sigma}^2_\omega$ across space. As an aside, a correlation between σ^2_ε and σ^2_ω across space would be unrelated to (and does not in any way invalidate) the assumption that intra- and intersubject errors are independent at each location in space (see Appendix).

As expected, GM masking led to smaller (~40%) ROIs with higher (~19%) mean CBF than SE-EPI masking. However, ROI-wise $\hat{\sigma}^2_\varepsilon$ obtained from SE-EPI masking showed no tendency to be smaller than that from GM masking. These results suggest that compared to GM masking, SE-EPI masks are less sensitive for CASL activation experiments. On the other hand, ROI-wise $\hat{\sigma}^2_\omega$ from SE-EPI masking was on average 25% (±8%) smaller than that from GM masking, which is consistent with the idea that most of the true intersubject variability in CBF comes from GM.

While power for a paired t-test (without Subject × Condition interactions, see Appendix) only depends on σ^2_ε, power for an independent sample t-test depends on both σ^2_ε and σ^2_ω. To determine which of the two dominates $\mathrm{var}\langle\hat{\mu}\rangle$ in an independent sample t-test we use the fact that when $n = \sigma^2_\varepsilon/\sigma^2_\omega$, the contributions of intra- and intersubject variances are equal; when $n > \sigma^2_\varepsilon/\sigma^2_\omega$, the intersubject variance is the dominating term (see Eq. (A6)). For GM masking, Table 1 shows a range of $\hat{\sigma}^2_\varepsilon/\hat{\sigma}^2_\omega$ from 3 to 98. Thus, when using any of these ROIs, for an independent sample t-test with $n > 98$, $\mathrm{var}\langle\hat{\mu}\rangle$ will be dominated by the intersubject variance.

For independent and identically distributed errors at each voxel, σ^2_ε should vary as the inverse of ROI size. However, σ^2_ω does not theoretically depend on MRI noise or any error that varies randomly across voxels, and therefore should not depend on ROI size. These predictions were borne out in Figs. 5A and B, respectively. Fig. 5A suggests that other sources of variability in addition to size contribute to ROI-wise $\hat{\sigma}^2_\varepsilon$. In particular, left BA 4 and left hippocampus ROIs were very similar in size (382 and 423 voxels, respectively), but ROI-wise $\hat{\sigma}^2_\varepsilon$ was 8.0 times larger for left BA 4 despite the mean CBF being similar [66.9 and 74.2 ml/(100 g min), respectively]. This was also true for the right hemisphere where ROI-wise $\hat{\sigma}^2_\varepsilon$ was 7.5 times larger for right BA 4 than for right hippocampus. As we discuss below, this difference can be explained by the increase of w with superior slices.

Power curves

Based on the variance values from GM masked ROIs (Table 1), estimated power curves for left hippocampus and left BA 4 are shown as a function of the number of subjects per group for an

Table 1
Estimated ROI-wise CASL CBF intra- and intersubject variances

ROI	Masking procedure	Average size	Average CBF	$\hat{\sigma}_{\varepsilon}^2$	$\hat{\sigma}_{\omega}^2$	$(\hat{\sigma}_{\varepsilon}^2/\hat{\sigma}_{\omega}^2)$
Right hippocampus	GM	405	73.7	2968	153	19.4
Right inferior frontal gyrus	GM	1973	74.3	5219	103	50.6
Right middle frontal gyrus	GM	2695	69.4	10553	236	44.7
Right occipital lobe	GM	4213	76.7	1549	439	3.5
Right precentral gyrus	GM	1235	71.1	11566	306	37.8
Right Brodman area 4	GM	386	64.8	22365	570	39.2
Right temporal lobe	GM	7475	76.2	1699	272	6.2
Left hippocampus	GM	423	74.2	3417	137	24.9
Left inferior frontal gyrus	GM	1794	74.2	5282	123	42.9
Left middle frontal gyrus	GM	2428	69.9	10914	270	40.4
Left occipital lobe	GM	4447	77.1	1686	444	3.8
Left precentral gyrus	GM	1185	70.6	12777	340	37.5
Left Brodman area 4	GM	382	66.9	27415	540	50.7
Left temporal lobe	GM	6981	74.5	1526	239	6.3
Right hippocampus	SE-EPI	548	69.3	2730	182	15.0
Right inferior frontal gyrus	SE-EPI	4731	62.6	4642	47	98.7
Right middle frontal gyrus	SE-EPI	7297	57.8	9302	141	65.9
Right occipital lobe	SE-EPI	10419	61.8	1599	286	5.6
Right precentral gyrus	SE-EPI	4169	56.4	14322	261	54.9
Right Brodman area 4	SE-EPI	1354	53.5	26218	551	47.6
Right temporal lobe	SE-EPI	16453	64.2	1895	161	11.8
Left hippocampus	SE-EPI	577	71.5	3451	139	24.8
Left inferior frontal gyrus	SE-EPI	4651	61.1	4448	67	66.4
Left middle frontal gyrus	SE-EPI	7302	56.2	9172	162	56.6
Left occipital lobe	SE-EPI	10303	64.9	1652	344	4.8
Left precentral gyrus	SE-EPI	4164	56.0	15066	261	57.7
Left Brodman area 4	SE-EPI	1276	55.6	30193	427	70.7
Left temporal lobe	SE-EPI	16414	62.4	1678	152	11.0

Units of ROI size are voxels (1 voxel = 8 $mm^3 = 8 \times 10^{-3}$ cm^3). Units of CBF are ml/(100 g min). Units of $\hat{\sigma}_{\varepsilon}^2$ and $\hat{\sigma}_{\omega}^2$ are CBF^2.

independent sample *t*-test (Fig. 6) and the total number of subjects for a paired *t*-test (Fig. 7). Each curve corresponds to a certain number of CBF images acquired per subject; μ was either 10 ml/(100 g min) (Figs. 6A, C and 7A, C) or 20 ml/(100 g min) (Figs. 6B, D and 7B, D). A consequence of both $\hat{\sigma}_{\varepsilon}^2$ and $\hat{\sigma}_{\omega}^2$ being larger for BA 4 than hippocampus is that power is substantially lower for BA 4 in all designs.

The hippocampus ROI exhibits acceptable power for an independent sample *t*-test at feasible clinical sample sizes and moderate effect sizes. For example, to obtain power = 0.90 when 100 CBF images are acquired per subject, an estimated <10 subjects per group would be needed to detect $\mu = 20$ ml/(100 g min) difference between groups. All other parameters being equal, for a small effect size of $\mu = 10$ ml/(100 g min) (i.e., a deviation of ~15% from

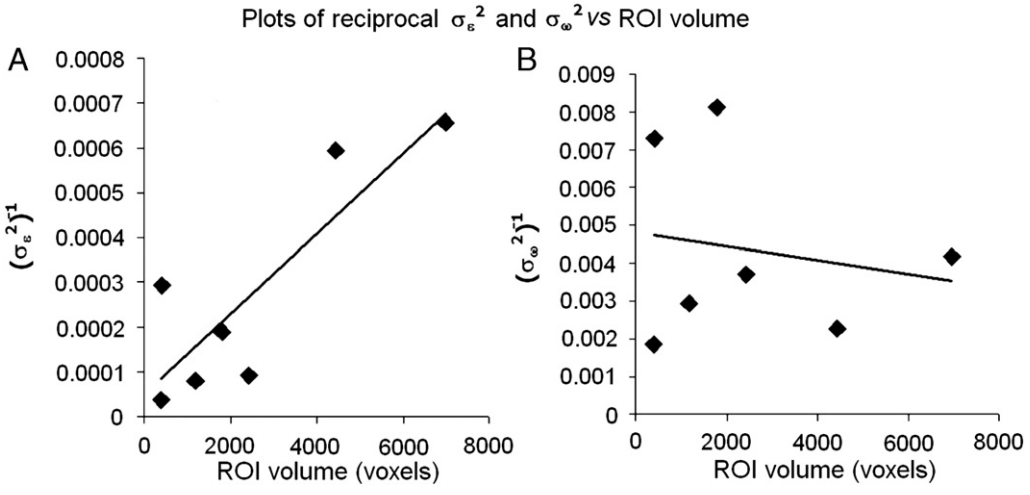

Fig. 5. (A) Plot of reciprocal $\hat{\sigma}_{\varepsilon}^{-2}$ versus GM ROI volume with best-fit line ($R^2 = 0.73$). (B) Plot of reciprocal $\hat{\sigma}_{\omega}^{-2}$ versus GM ROI volume with best-fit line ($R^2 = 0.03$). Only data from left hemisphere GM ROIs are plotted. Results (not shown) are very similar for right hemisphere ROIs and ROIs using SE-EPI masking.

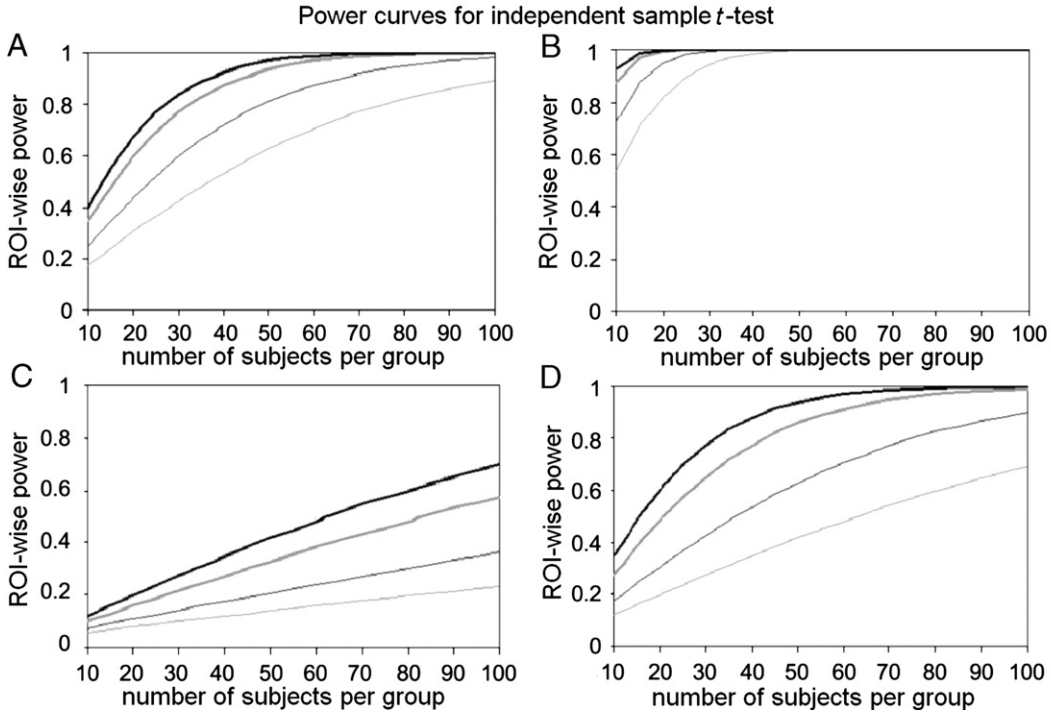

Fig. 6. Independent sample *t*-test design power curves for selected effect sizes and GM ROIs. (A) Left hippocampus, $\mu = 10$ ml/(100 g min). (B) Left hippocampus, $\mu = 20$ ml/(100 g min). (C) Left BA 4, $\mu = 10$ ml/(100 g min). (D) Left BA 4, $\mu = 20$ ml/(100 g min). Moving upward, each curve corresponds to an increasing number of CBF images per subject starting with 10 (thin gray line), 20 (thin black line), 50 (thick gray line), and 100 (thick black line).

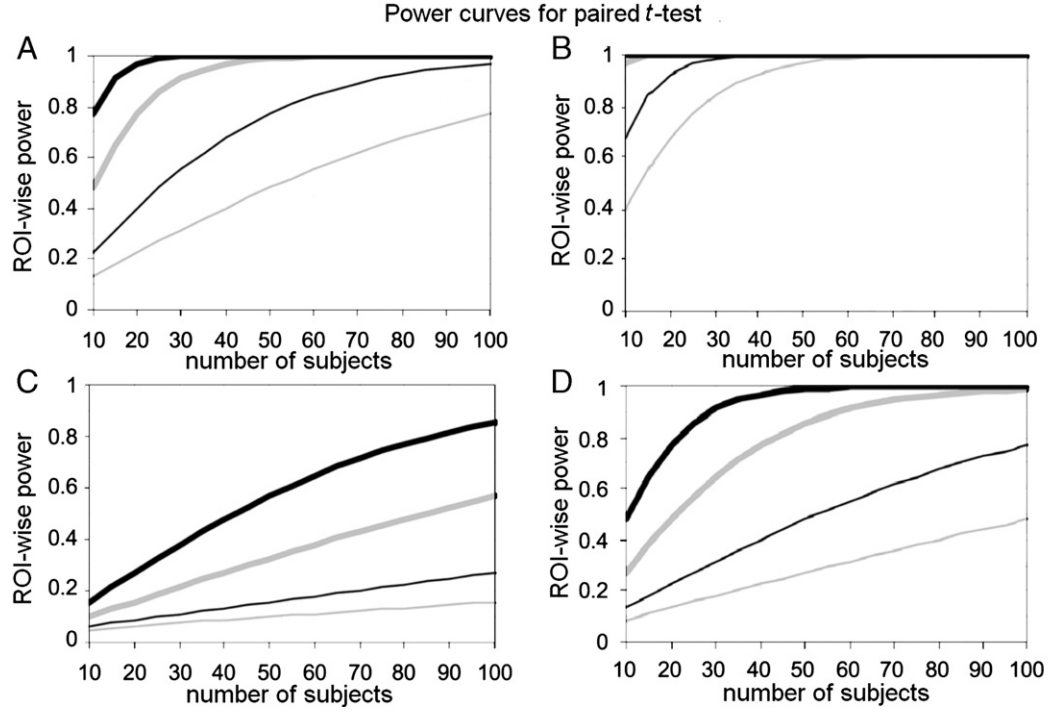

Fig. 7. Paired *t*-test design power curves for selected effect sizes and GM ROIs. (A) Left hippocampus, $\mu = 10$ ml/(100 g min). (B) Left hippocampus, $\mu = 20$ ml/(100 g min). (C) Left BA 4, $\mu = 10$ ml/(100 g min). (D) Left BA 4, $\mu = 20$ ml/(100 g min). Moving upward, each plot corresponds to an increasing number of CBF images per subject starting with 10 (thin gray line), 20 (thin black line), 50 (thick gray line), and 100 (thick black line). The number of CBF images per condition equals half that per subject. α equals two-tailed 0.05 for all plots.

normal hippocampal CBF), 36 subjects per group would be needed. This example provides a sense of the practical limits of sensitivity of CASL to detect group differences in resting CBF.

A concrete example of a paired *t*-test for neuroimaging would be an experiment in which a finger tapping condition is compared, within subject, to a resting condition. Fig. 7D indicates that in BA 4 for μ=20 ml/(100 g min), to obtain power=0.80 with 50 CBF images acquired per condition (i.e., 100 images per subject), an estimated 22 subjects would be needed.

Discussion

We have estimated intra- and intersubject variances of CASL CBF measurements in GM from several neuroanatomically defined ROIs for an elderly population. SE-EPI acquisition was used, thus minimizing signal dropout due to susceptibility effects. We restricted our analysis to GM as this tissue is of greater interest in the context of brain metabolism. Our GM CBF estimates are biased downwards due to partial volume effects. However, we do not expect this bias to be large because our GM ROIs included only voxels that were expected to be 80% or more GM. Donahue et al. (2006) measured the error induced in GM CBF estimates by partial volume effects at 3T and found it to be 10–20%.

Using these results and the relevant equations (see Appendix), power can be estimated for any of the ROIs with any desired μ, n, N, and α. We have also provided explicit power curves for BA 4 and hippocampus, which are especially relevant for studies of motor execution and AD, respectively.

While the emphasis of this study was the sensitivity of CASL CBF in general, the specific population studied was that of normal, elderly subjects. The results are therefore directly relevant for the design of CASL CBF experiments to study AD and other age-related diseases, as well as normal aging. However, if one surmises that σ_ε^2 and σ_ω^2 are similar between different populations, the results obtained here would be qualitatively germane for other populations. We conjecture that both σ_ε^2 and σ_ω^2 are larger in elderly than young because of potentially increased motion (which would impact σ_ε^2) and increased intersubject variability in subclinical aged-related pathology (which would impact σ_ω^2) in elderly.

σ_ε^2 reflects all sources of MR scanner noise, which would include Johnson noise (thermally mediated random variation in voltage across a resistor) from the subject load (and to some extent the RF coil), as well as head motion and physiological noise such as that due to cardiac pulsatility or even random neurogenic CBF fluctuations. For the designs to yield exact *t*-statistics, the σ_ε^2 values need to be the same across subjects. Inspection of distributions of $\hat{\sigma}_\varepsilon^2$ for BA 4 and hippocampus suggested that this was not the case, as they did not conform well to a χ^2 density with N'-1 degrees of freedom (data not shown). Even in the extreme, non-identical σ_ε^2 across subjects would not bias the estimation of var$\langle\hat{\mu}\rangle$ (see Appendix), but instead would invalidate the use of the *t*-distribution and consequently invalidate the power analysis. However, the distribution of the ROI-wise averages for BA 4 and hippocampus was approximated well as normal, therefore concern about validity of *t*-tests and corresponding power analyses is mitigated. The apparent heterogeneity of $\hat{\sigma}_\varepsilon^2$ does, however, suggest the use of weighted least square estimation on CASL CBF to improve sensitivity.

There was a substantial variation in $\hat{\sigma}_\varepsilon^2$ between ROIs that could not be explained simply by ROI volume. For example, BA 4 ROI-wise $\hat{\sigma}_\varepsilon^2$ was ~8 times larger than that of hippocampus, despite the ROIs being very similar in size. One mechanism theoretically expected to affect σ_ε^2 through the acquisition slice is the effective post-labeling delay, *w*. The amount of label diminishes during *w* through T_1 relaxation, which, for a given CBF and for an ascending acquisition, should lead to a smaller percent change signal in more superior slices. This decrease should not lead to a smaller estimated CBF as *w* is explicitly accounted for in the physical model (Eq. (1)). It also should not affect the intrasubject variance of percent change signal assuming noise is additive and not multiplicative to MR signal. However, this decrease should result in an increased σ_ε^2 because, for a given CBF, the smaller the CASL percent change signal, the larger the multiplicative factor used to transform this signal to flow, and therefore the larger the σ_ε^2 inflation. Indeed, ancillary analyses confirmed that *w* explains most of the difference in $\hat{\sigma}_\varepsilon^2$ between BA 4 and hippocampus (data not shown). Furthermore, the maps of σ_ω^2 showed greater values as one moved superiorly, as would be expected under this PLD effect.

One might conjecture that in studies where superior slices are of interest, the aforementioned *w* effect could be obviated by acquiring them with shorter *w*. However, as the validity of the CBF model used assumes $w>\delta_a$, the minimum required *w* increases as slice position moves superiorly. Therefore, to fully eliminate relaxation related sensitivity loss at superior slices, one would have to reduce δ_a by placing the labeling plane as close to the slice as saturation effects and adiabatic conditions permit. However, the positioning of labeling plane is restricted in applications where whole brain coverage is needed.

In a single elderly subject, for each slice, we estimated arterial transit time, δ_a, ranging from 0.33 to 1.07 s, corresponding to an average 122ms/cm or a *z*-velocity an average *z*-velocity of spins of ~8 cm/s. These estimates are in good agreement with literature values for arterial transit time in GM in various regions of the brain: 0.6–1.2 s by Gonzalez-At et al. (2000)., 0.73–0.97 s by Yang et al. (2000). In our sequence, *w* was at least 0.5 s longer than δ_a for each slice. Although there is conceivably a distribution of δ_a among the elderly population, we conjecture that $w>\delta_a$ in a large proportion of the non-diseased elderly population. Further work is needed to establish the effect of age in arterial transit times. Furthermore, by comparing CBF in the same slice at a given *w* for both acquisition orders, we showed that our implementation of CASL CBF was independent of the acquisition order. Together, these results suggest that saturation of labeled spins (which would be expected if $w<\delta_a$) was not appreciable. However, the presence of some intravascular signal (Fig. 1B) indicates that the assumption $w>\delta_a$ was most likely not met by all the subjects.

Floyd et al. (2003) measured intrasubject variance of CASL CBF at 1.5 T using ascending acquisition in ROIs defined by vascular territories. Instead of using time series variance to define intrasubject variance, they used the variation in ROI means between runs (n'=45 CBF images/run) separated by either 1 h or 1 week. Therefore, if resting CBF varies substantially over time within subjects, Floyd et al.'s estimates would include sources of variation that in our analysis were absorbed implicitly by σ_ω^2. However, in the approximation of stable CBF over time, their measure of intrasubject variance, "*w*SD", should equal $\sqrt{\sigma_\varepsilon^2/45}$. Their reported range (over ROIs) for *w*SD for the 1-h data was 3.0–9.1 ml/(100 g min) and for the 1-week data was 6.8–8.7 ml/(100 g min) with a median of 7.4 in both cases. These ranges of ROI-wise *w*SD overlap with those of the current study [GM masked ROIs *w*SD range: 5.8–24.7 ml/(100 g min), median=10.8;

SE-EPI masked ROIs *w*SD range: 6.0–25.9 ml/(100 g min), median = 10.0]. As Floyd et al. did not report ROI volumes, a more direct comparison to our values is not possible. However, considering that the ROIs used in Floyd et al. covered entire perfusion territories, it is likely that they were larger than the neuroanatomical ROIs used in our study.

Yen et al. (2002) reported variance of PASL CBF at 1.5 T from GM ROI in a single slice. ROI size across subjects varied from 50 to 80 cm^3, similar in size to our hippocampal and BA 4 ROIs. We calculated *w*SD from the results of Yen et al. and it was 4.1, which is ~2 and 6 times smaller than that of our hippocampal and BA 4 ROIs, respectively. In contrast, σ_ω^2 from Yen et al. was 114 $[ml/(100\ g\ min)]^2$, which lies within the range of our ROI-wise results.

σ_ω^2 reflects the variation between subjects in the CASL CBF in the absence of intrasubject error. Contributions to σ_ω^2 theoretically include variation in neuronal/neuropil/glial density, baseline neuronal metabolism, blood T_1 due to differences in hematocrit content, hormonal levels, and metabolic–vascular coupling which in turn could be affected by within-population pathological variation, developmental differences, and other aspects of genotypic variation. Other, non-physiological sources of variation such as subject-specific misspecification of transit time and/or other MR/physiologic parameters would also contribute to σ_ω^2. Furthermore, any within-subjects variation in CBF over long time scales would also implicitly contribute to our σ_ω^2; however, this type of variation over 1 week has been shown to be insubstantial (Floyd et al., 2003). Though we did not rigorously quantitate differences in σ_ω^2 between GM and WM, the estimated map of σ_ω^2 (Fig. 1D) suggests that it is larger in GM than in WM, which, if true, would imply that physiological CBF variation is greater in GM.

Recently, implementations of CASL at higher fields have been reported (Wang et al., 2002; Wang et al., 2005a; Wang et al., 2005b). Presently, there have been no empirical studies that explicitly address the effect of B_o on sensitivity for CASL. Theoretically, however, ASL signal is expected to increase with B_o due to two main factors: an inherent increase in MR SNR with B_o and a longer longitudinal relaxation time of labeled arterial water (Golay and Petersen, 2006). Wang et al. (2002) have provided a theoretical framework for the dependence of ASL signal with B_o. They found that in the absence of T_2* effect (appropriate for SE-EPI), CASL SNR is expected to an ~3× increase at 3 T compared to 1.5 T, which should correspond to an ~9× decrease in σ_ε^2 if thermal noise dominates physiological noise in CBF time series.

Using gradient echo EPI, Wang et al. (2005b) have reported that compared to a standard volume coil, an 8-channel array coil with (2-fold) and without acceleration provided a 45% and 56% decrease in intrasubject standard deviation, respectively. These effects could conceivably be different for a SE acquisition where susceptibility effects are less.

Although, σ_ε^2 depends on pulse sequence and hardware characteristics, the CASL implementation used in this study is the most commonly used (Golay et al., 2004) and as such the results presented here should be quite useful in a variety of applications for CASL in the elderly population. Furthermore, the data presented here can still be useful for other CASL implementations assuming theoretical predictions about changes in SNR can be made. For example, if SNR at 3 T is 3 times of that at 1.5 T (Wang et al., 2002) then, all other parameters being equal, the σ_ε^2 estimates reported here could be reduced 9-fold for power calculations for the desired design. The same logic holds for post-processing techniques that aim at reducing σ_ε^2 (Restom et al., 2006). In contrast, σ_ω^2 should not be affected appreciably by B_o, coil implementation, pulse sequence, or post-processing strategy. Even more fundamentally, σ_ω^2 is, theoretically, method-independent and should therefore be the same for CASL, PASL, and even other non-MRI imaging techniques such as PET.

We presented estimates of σ_ε^2 and σ_ω^2 using a particular CASL physiological model (Wang et al., 2002). The use of other models would, to a first approximation, preserve the ratio of mean to standard deviation. Therefore, the current results could be used to perform power analyses for effect sizes expressed as percentages of the resting ROI CBF means (instead of CBF units) in an approximately model-free manner.

Because our study involved the measurement of only one condition, rest, a Subject × Condition variance term (see Appendix) could not be estimated. Therefore the paired *t*-test model we used was based on the assumption that the variance of $\hat{\mu}$ depends only on σ_ε^2 and not on an additional variance term associated with a Subject × Condition interaction. If incorrect, this assumption would introduce an additional source of physiological variability into the estimation for this design, and effectively make the power analysis presented for paired *t*-test relevant only for "fixed effects" inference. That is, inference valid only for the particular set of subjects sampled, and not the population from which they were sampled (Friston et al., 2005). The quantitative effect of ignoring this term in the context of paired *t*-test depends on its actual magnitude relative to σ_ε^2. For now, one can consider the paired *t*-test power analysis we present here to be correct for fixed effects inference, and potentially too lenient (i.e., leading to an over-estimation of power) for population-level (or "random effects") inference.

The elderly population under study was screened to exclude stroke (Sacco et al., 2004) but included individuals with diabetes, heart disease, and other diseases at standard prevalence rates (DeCarli et al., 2005). Although the definition of what is considered "healthy" for the elderly population is under clinical debate (DeCarli et al., 2005), possibly a more homogenously healthy population would exhibit smaller σ_ω^2. The CASL power estimates presented here should nevertheless prove useful and relevant in designing experiments in elderly subjects.

Acknowledgments

This work was supported by grants from the National Institute of Neurological Disorders and Stroke R01 NS 29993 and K12 RR 176548. Eric Zarahn was supported by a NARSAD Young Investigator Award. The first author expresses deepest gratitude to Barbara Cummings for her crucial support.

Appendix A. Power analysis

Power is equal to the integral of the probability density function (pdf) of the test statistic under a given alternative hypothesis with the lower limit of integration L being determined at least in part by the statistical threshold chosen to control type I error. For both independent samples and paired *t*-tests, assuming normal errors, the correct pdf to integrate is the non-central *t*. However, for simplicity the standard normal pdf was used:

$$\text{power}(L) \approx \frac{1}{\sqrt{2\pi}} \int_{L(\mu,\mathbf{d})}^{\infty} e^{\frac{-x^2}{2}} dx \tag{A1}$$

where **d** is an abstract vector parameter representing experimental design [number of subjects, nature of effects (within or between subjects), pulse sequence parameters, etc.], and L is

$$L(\mu,\mathbf{d}) = z_{\alpha/2} - \frac{\mu}{\sqrt{\mathrm{var}\langle\hat{\mu}\rangle}} \tag{A2}$$

where $z_{\alpha/2}$ is the upper threshold corresponding to a two-tailed type I error rate of α, and $\mathrm{var}\langle\hat{\mu}\rangle$ is the variance of $\hat{\mu}$ (the ordinary least squares estimator of the effect size, μ, which is the CBF value being tested against 0 in either experimental design).

Let y_{hijk} be the CASL CBF observation at a given voxel or ROI from group h, condition i, subject j, and replication k. A univariate statistical model for y_{hijk} is

$$y_{hijk} = \mu_{hi} + \omega_j + \eta_{ij} + \varepsilon_{hijk} \tag{A3}$$

where μ_{hi} is the true CBF for condition i in group h. The normally distributed intersubject errors ω_j have variance σ^2_ω. The normally distributed time series errors ε_{hijk} are assumed to be independent with identical variance σ^2_ε, which does not depend on j. ω_j and ε_{hijk} are assumed to be independent (if they were not, then time series error would somehow "know" to be correlated with subject-wise variation in CBF). For completeness, [A3] includes the Subject × Condition interaction term η_{ij}. If data were acquired over both conditions of a paired t-test, then a σ^2_η could be estimated, which would contribute to $\mathrm{var}\langle\hat{\mu}\rangle$. However, we only acquired data for one condition, and so we cannot estimate a σ^2_η, therefore our paired t-test inference is formally valid only for fixed effects inference.

For an independent sample t-test, let $\mu=\mu_{1i}-\mu_{2i}$. Then, $\hat{\mu}=y_{1i..}-y_{2i..}$, where:

$$y_{hi..} = \frac{\sum_{j=1}^{N} y_{hij.}}{N} \tag{A4}$$

$$y_{hij.} = \frac{\sum_{k=1}^{n} y_{hijk}}{n} \tag{A5}$$

with N and n denoting the number of subjects per group and the number of observations per subject, respectively. The variance of $\hat{\mu}$ is:

$$\mathrm{var}\langle\hat{\mu}\rangle = 2\cdot\frac{\left(\sigma^2_\omega + \frac{\sigma^2_\varepsilon}{n}\right)}{N}. \tag{A6}$$

For a paired t-test, let $\mu = \mu_{h1}-\mu_{h2}$ and $\hat{\mu}=y_{h1..}-y_{h2..}$. The fixed effect variance of $\hat{\mu}$ is:

$$\mathrm{var}\langle\hat{\mu}\rangle = 4\cdot\frac{\sigma^2_\varepsilon}{n\cdot N} \tag{A7}$$

where N is the number of subjects and n is the total number of observations per subject (i.e., the number of observations per subject per condition is $n/2$).

σ^2_ε and σ^2_ω can be estimated from a random sample of N' subjects with n' observations per subject from condition i. The estimate of σ^2_ε in the jth subject is

$$\hat{\sigma}^2_{\varepsilon,j} = \frac{\sum_{k=1}^{n'}\left(y_{hijk}-y_{hij.}\right)^2}{n'-1} \tag{A8}$$

Since we assume $E\langle\hat{\sigma}^2_{\varepsilon,j}\rangle$ does not depend on j, $\hat{\sigma}^2_{\varepsilon,i}$ can be pooled over the N' subjects to provide a better estimate:

$$\hat{\sigma}^2_\varepsilon = \frac{\sum_{j=1}^{N'}\hat{\sigma}^2_{\varepsilon,j}}{N'} \tag{A9}$$

σ^2_ω can be estimated as a weighted difference between the sample variance of $\{y_{hi1.}, y_{hi2.}, \ldots y_{hiN'.}\}$ and $\hat{\sigma}^2_\varepsilon$:

$$\hat{\sigma}^2_\omega = \frac{\sum_{j=1}^{N'}\left(y_{hij.}-y_{hi..}\right)^2}{N'-1} - \frac{\hat{\sigma}^2_\varepsilon}{n'} \tag{A10}$$

$\hat{\sigma}^2_\varepsilon$ and $\hat{\sigma}^2_\omega$ can be substituted into Eqs. (A6) and (A7) to provide an unbiased estimator of $\mathrm{var}\langle\hat{\mu}\rangle$.

References

Alsop, D.C., Detre, J.A., 1996. Reduced transit-time sensitivity in non-invasive magnetic resonance imaging of human cerebral blood flow. J. Cereb. Blood Flow Metab. 16, 1236–1249.

Alsop, D.C., Detre, J.A., 1998. Multisection cerebral blood flow MR imaging with continuous arterial spin labeling. Radiology 208, 410–416.

Alsop, D.C., Detre, J.A., Grossman, M., 2000. Assessment of cerebral blood flow in Alzheimer's disease by spin-labeled magnetic resonance imaging. Ann Neurol 47, 93–100.

Brunet, E., Sarfati, Y., Hardy-Bayle, M.C., Decety, J., 2003. Abnormalities of brain function during a nonverbal theory of mind task in schizophrenia. Neuropsychologia 41, 1574–1582.

Buxton, R.B., Frank, L.R., Wong, E.C., Siewert, B., Warach, S., Edelman, R.R., 1998. A general kinetic model for quantitative perfusion imaging with arterial spin labeling. Magn Reson Med 40, 383–396.

DeCarli, C., Massaro, J., Harvey, D., Hald, J., Tullberg, M., Au, R., Beiser, A., D'Agostino, R., Wolf, P.A., 2005. Measures of brain morphology and infarction in the Framingham Heart Study: establishing what is normal. Neurobiol Aging 26, 491–510.

Dieterich, M., Bartenstein, P., Spiegel, S., Bense, S., Schwaiger, M., Brandt, T., 2005. Thalamic infarctions cause side-specific suppression of vestibular cortex activations. Brain 128, 2052–2067.

Donahue, M.J., Lu, H., Jones, C.K., Pekar, J.J., van Zijl, P.C., 2006. An account of the discrepancy between MRI and PET cerebral blood flow measures. A high-field MRI investigation. NMR Biomed 19, 1043–1054.

Floyd, T.F., Ratcliffe, S.J., Wang, J., Resch, B., Detre, J.A., 2003. Precision of the CASL-perfusion MRI technique for the measurement of cerebral blood flow in whole brain and vascular territories. J Magn Reson Imaging 18, 649–655.

Friston, K.J., Stephan, K.E., Lund, T.E., Morcom, A., Kiebel, S., 2005. Mixed-effects and fMRI studies. Neuroimage 24, 244–252.

Golay, X., Petersen, E.T., 2006. Arterial spin labeling: benefits and pitfalls of high magnetic field. Neuroimaging Clin. N. Am. 16, 259–268, x.

Golay, X., Hendrikse, J., Lim, T.C., 2004. Perfusion imaging using arterial spin labeling. Top Magn Reson Imaging 15, 10–27.

Gonzalez-At, J.B., Alsop, D.C., Detre, J.A., 2000. Cerebral perfusion and arterial transit time changes during task activation determined with continuous arterial spin labeling. Magn Reson Med 43, 739–746.

Kety, S.S., Schmidt, C.F., 1948. The nitrous oxide method for the quantitative determination of cerebral blood flow in man: theory. Procedure and Normal Values. J Clin Invest 27, 476–483.

Kim, S.G., Ugurbil, K., 1997. Comparison of blood oxygenation and cerebral blood flow effects in fMRI: estimation of relative oxygen consumption change. Magn Reson Med 38, 59–65.

Kudo, K., Terae, S., Katoh, C., Oka, M., Shiga, T., Tamaki, N., Miyasaka, K., 2003. Quantitative cerebral blood flow measurement with dynamic perfusion CT using the vascular-pixel elimination method: comparison

with $H_2(15)O$ positron emission tomography. AJNR Am J Neuroradiol 24, 419–426.
Maldjian, J.A., Laurienti, P.J., Kraft, R.A., Burdette, J.H., 2003. An automated method for neuroanatomic and cytoarchitectonic atlas-based interrogation of fMRI data sets. Neuroimage 19, 1233–1239.
Maldjian, J.A., Laurienti, P.J., Burdette, J.H., 2004. Precentral gyrus discrepancy in electronic versions of the Talairach atlas. Neuroimage 21, 450–455.
Mildner, T., Moller, H.E., Driesel, W., Norris, D.G., Trampel, R., 2005. Continuous arterial spin labeling at the human common carotid artery: the influence of transit times. NMR Biomed 18, 19–23.
Restom, K., Behzadi, Y., Liu, T.T., 2006. Physiological noise reduction for arterial spin labeling functional MRI. Neuroimage 31, 1104–1115.
Sacco, R.L., Anand, K., Lee, H.S., Boden-Albala, B., Stabler, S., Allen, R., Paik, M.C., 2004. Homocysteine and the risk of ischemic stroke in a triethnic cohort: the Northern Manhattan Study. Stroke 35, 2263–2269.
Scarmeas, N., Habeck, C.G., Zarahn, E., Anderson, K.E., Park, A., Hilton, J., Pelton, G.H., Tabert, M.H., Honig, L.S., Moeller, J.R., Devanand, D.P., Stern, Y., 2004. Covariance PET patterns in early Alzheimer's disease and subjects with cognitive impairment but no dementia: utility in group discrimination and correlations with functional performance. Neuroimage 23, 35–45.
Talairach, J.a.T.P., 1988. Co-Planar Stereotaxic Atlas of the Human Brain (Thieme, Stuttgart, Germany).
Tzourio-Mazoyer, N., Landeau, B., Papathanassiou, D., Crivello, F., Etard, O., Delcroix, N., Mazoyer, B., Joliot, M., 2002. Automated anatomical labeling of activations in SPM using a macroscopic anatomical parcellation of the MNI MRI single-subject brain. Neuroimage 15, 273–289.
Wang, J., Alsop, D.C., Li, L., Listerud, J., Gonzalez-At, J.B., Schnall, M.D., Detre, J.A., 2002. Comparison of quantitative perfusion imaging using arterial spin labeling at 1.5 and 4.0 Tesla. Magn Reson Med 48, 242–254.
Wang, J., Aguirre, G.K., Kimberg, D.Y., Roc, A.C., Li, L., Detre, J.A., 2003a. Arterial spin labeling perfusion fMRI with very low task frequency. Magn Reson Med 49, 796–802.
Wang, J., Alsop, D.C., Song, H.K., Maldjian, J.A., Tang, K., Salvucci, A.E., Detre, J.A., 2003b. Arterial transit time imaging with flow encoding arterial spin tagging (FEAST). Magn Reson Med 50, 599–607.
Wang, J., Zhang, Y., Wolf, R.L., Roc, A.C., Alsop, D.C., Detre, J.A., 2005a. Amplitude-modulated continuous arterial spin-labeling 3.0-T perfusion MR imaging with a single coil: feasibility study. Radiology 235, 218–228.
Wang, Z., Wang, J., Connick, T.J., Wetmore, G.S., Detre, J.A., 2005b. Continuous ASL (CASL) perfusion MRI with an array coil and parallel imaging at 3T. Magn. Reson. Med. 54, 732–737.
Werner, R., Norris, D.G., Alfke, K., Mehdorn, H.M., Jansen, O., 2005. Improving the amplitude-modulated control experiment for multislice continuous arterial spin labeling. Magn. Reson. Med. 53, 1096–1102.
Yang, Y., Engelien, W., Xu, S., Gu, H., Silbersweig, D.A., Stern, E., 2000. Transit time, trailing time, and cerebral blood flow during brain activation: measurement using multislice, pulsed spin-labeling perfusion imaging. Magn. Reson. Med. 44, 680–685.
Yen, Y.F., Field, A.S., Martin, E.M., Ari, N., Burdette, J.H., Moody, D.M., Takahashi, A.M., 2002. Test–retest reproducibility of quantitative CBF measurements using FAIR perfusion MRI and acetazolamide challenge. Magn. Reson. Med. 47, 921–928.
Zarahn, E., Slifstein, M., 2001. A reference effect approach for power analysis in fMRI. Neuroimage 14, 768–779.